Separation and Purification Technology 361 (2025) 131597

Contents lists available at ScienceDirect

Separation and Purification Technology

journal homepage: www.elsevier.com/locate/seppur

CuCo carbon aerogel as a bifunctional cathode for Electro-Fenton processes: Unveiling synergistic effects and catalytic mechanisms

Qian Ye [a], Timothy N. Hunter [b,*], Hao Xu [c], David Harbottle [b], Girish M. Kale [b], Martin R. Tillotson [a,*]

[a] School of Civil Engineering, University of Leeds, Leeds LS2 9JT, UK
[b] School of Chemical and Process Engineering, University of Leeds, Leeds LS2 9JT, UK
[c] Environment and Sustainability Institute, Faculty of Environment, Science and Economy, University of Exeter, Penryn Campus, Penryn TR10 9FE, UK

ARTICLE INFO

Editor: G. Chen

Keywords:
Oxygen reduction activity
CuCo carbon aerogel
Tetracycline
Electro-Fenton process
Synergistic effect
Reactive species

ABSTRACT

Combining electrocatalytic oxygen reduction reaction (ORR) and heterogeneous electro-Fenton (HEF) reaction is considered a promising approach for generating reactive radicals to decompose organic micropollutants in water. A novel catalyst, copper-cobalt carbon aerogel (CuCo/CA), was successfully fabricated and directly applied as a bifunctional cathode in an HEF system. The synergistic effect of Cu and Co contributed to the development of distinctive microstructures, including abundant oxygen-containing groups, carbon defects, a large surface area and a unique porous structure. These structural features endowed CuCo/CA with rapid electron transfer capability and enhanced activity and selectivity for the two-electron ORR process. In the constructed EF system, CuCo/CA achieved its dual functionality by catalysing the electrosynthesis of hydrogen peroxide and its *in situ* activation to generate highly reactive hydroxyl radicals. Notably, anodic oxygen evolution in the system eliminated the need for additional oxygen input, enhancing its cost-effectiveness. The system demonstrated degradation ability for a range of candidate organic pollutants, including antibiotics, analgesics, organic acid and dye. After six consecutive runs, CuCo/CA EF system achieved satisfactory TC removal and good adaptability within a broad pH range. Long-term stability and low electricity consumption highlighted the potential of CuCo/CA as an efficient and sustainable cathode in EF technology for water decontamination.

1. Introduction

Inefficient biodegradation of antibiotics has classified them as persistent organic pollutants (POPs) in the environment [1]. Tetracycline (TC), a commonly used antibiotic, frequently contaminates water bodies, harming plant growth, aquatic ecosystems, and microbial communities [2]. TC is frequently detected in water bodies such as surface water, drinking water and wastewater [3]. As a result, the need for effective removal methods is increasing. The Electro-Fenton (EF) process, which generates reactive hydroxyl radicals (·OH) for pollutant oxidation, is a promising advanced oxidation process (AOP) for breaking down these persistent compounds [4].

In EF systems, hydrogen peroxide (H_2O_2) is generated *in situ via* a two-electron oxygen reduction reaction (ORR, Equation (1)) at the cathode, avoiding risks of H_2O_2 transportation and handling compared to classic Fenton system [5]. Subsequently, ·OH radicals are produced through the activation of H_2O_2 by Fe^{2+} (Equation (2)) [6], effectively decomposing various organics via non-selective oxidation. However, homogeneous EF systems are limited by pH constraints (typically below 4) and require continuous Fe^{2+} addition [4]. Therefore, integrated cathode materials with dual functionalities, including two-electron ORR and *in situ* H_2O_2 activation, hold significant application potential. In such systems, electro-activation of H_2O_2 to ·OH depends on a one-electron redox cycle occurring at exposed active sites of the cathode, which eliminates the need for Fe^{2+} and widens applicable pH range [7].

$$O_2 + 2H^+ + 2e^- \rightarrow H_2O_2 \quad (1)$$

$$Fe^{2+} + H_2O_2 \rightarrow Fe^{3+} + OH^- + \bullet OH \quad (2)$$

Ensuring high ·OH production efficiency in the hetero-EF reaction requires a catalyst that can selectively catalyse H_2O_2 generation *via* a two-electron pathway and subsequently activates H_2O_2 to yield ·OH. Previous studies have highlighted hetero-EF activity of ·OH production in materials such as a magnetite/multiwalled carbon nanotubes [8],

* Corresponding authors.
E-mail addresses: T.N.Hunter@leeds.ac.uk (T.N. Hunter), M.R.Tillotson@leeds.ac.uk (M.R. Tillotson).

https://doi.org/10.1016/j.seppur.2025.131597
Received 20 November 2024; Received in revised form 3 January 2025; Accepted 10 January 2025
Available online 11 January 2025

defective three-dimensional porous carbon [9], and carbon nanofibers [10]. However, achieving rapid electro generation of ·OH remains challenging due to the difficulty in synchronizing efficient catalysis of both selective generation and activation of H_2O_2 into ·OH on a single electrocatalyst. It has been reported that a multi-component combination of transition metals with carbon composite catalysts has the potential to enhance electrochemical activity by regulating individual metal activity, thus further improving overall performance [11]. Catalysts synthesised through synergistic interaction of copper (Cu) and cobalt (Co) find extensive applications in various fields, including supercapacitors [12], Zn–air batteries [13], and electrochemical sensors [14]. Incorporation of Cu and Co species has been demonstrated to enhance electrochemical performance, such as specific capacity and cycling stability. Cu is regarded as one of the most crucial iron-free catalysts in Fenton-like systems. Copper ions (Cu^+) have a higher reaction rate ($k = 1 \times 10^4\ M^{-1}s^{-1}$) with H_2O_2 (Equation (3) compared to Fe^{2+} ($k = 76\ M^{-1}s^{-1}$) and can function effectively within a broad pH range [15]. Additionally, the Co^{2+}/Co^{3+} pair offers a stable redox potential, while Co^{2+} species in solution and on the surface exhibit great potential in the H_2O_2-mediated degradation of organic pollutants [16].

$$Cu^+ + H_2O_2 \rightarrow Cu^{2+} + OH^- + \bullet OH \quad (3)$$

To enhance electrocatalytic activity, a variety of carbon-based materials are employed in electrode fabrication including carbon felt [17], carbon aerogel [18], and graphite felt (GF) [19]. Among them, carbon aerogel (CA), distinguished by its 3D network structure, good electrical conductivity, and high surface area, emerges as an outstanding candidate for electrode construction [20]. In addition, carbon aerogel may also serve as a support for metal or metal oxide catalysts. The 3D network structure of CA increases active sites of the catalysts, and its adsorption capacity raises pollutant concentrations around these sites, leading to enhanced catalytic activity [18]. So far, the synergistic effects of Cu and Co on microstructures, electrochemical properties, and catalytic performances of CA have not been systematically revealed, and application of bimetallic carbon aerogel as an efficient electrode material for water decontamination remains to be further investigated.

In this work, a CuCo carbon aerogel (CuCo/CA) was synthesised as a bifunctional cathode in a hetero-EF system. The cathode microstructure, such as surface morphology, porosity, and chemical composition of CuCo/CA was analysed and compared with those of Cu/CA, Co/CA and pure CA. The synergistic effects of Cu and Co on regulating microstructure, enhancing ORR activity and selectivity and improving electrocatalytic ability were systematically investigated. This system simultaneously generates and activates H_2O_2 *in situ* without external aeration. Reaction parameters were optimised and radical generation mechanisms were revealed using TC as a model pollutant. Recyclability of CuCo/CA was investigated in six consecutive runs while long-term stability was evaluated in a continuous stirred tank reactor (CSTR). Finally, the extensively catalytic properties were further assessed using various organic contaminants.

2. Experimental section

Details of chemicals, cathode synthesis, and analytical methods are listed in Text S1 ~ S3 of the Electronic Supplementary Materials (ESM).

2.1. Cathode synthesis

Referring to the fabrication methodology of bimetallic carbon aerogel in our previous work [21], synthesis of CuCo/CA cathode (molar ratio of Cu:Co is 1:1) comprised of four stages: Gelation, solvent exchange, drying, and carbonization. Fig. 1 illustrates the schematic diagram of synthesis process. The synthesis details are clarified in Text S2 of the ESM.

2.2. Electrochemical degradation

Electrochemical degradations were performed within an undivided electrochemical cell (150 mL), in which the platinum sheet (4 cm^2) and synthesised carbon aerogels (CuCo/CA, Cu/CA, Co/CA and pure CA, 4.5 cm^2) were employed 2 cm away as the anode and cathode, respectively. The simulated pollutant solution comprised of 10 mg/L tetracycline (TC) and 0.05 mol/L Na_2SO_4 (as electrolyte) with Milli-Q^{TM} water (Merck Millipore), stirred with a magnetic bar at 400 rpm (25℃). For electro-Fenton (EF) systems, a DC power supply (Velleman 70–0768), configured for the operating current of the electrocatalytic reaction, was connected to the cathode and anode, and a constant current mode was used. No additional aeration was provided in most electro-Fenton reactions, while compressed air cylinders were utilized to evaluate the impact of various aeration rates. For electro-sorption (ES) systems, 1 mA of current with a flowing nitrogen (N_2) atmosphere of 0.2 L/min was maintained during reaction, and the solution was aerated with N_2 for 20

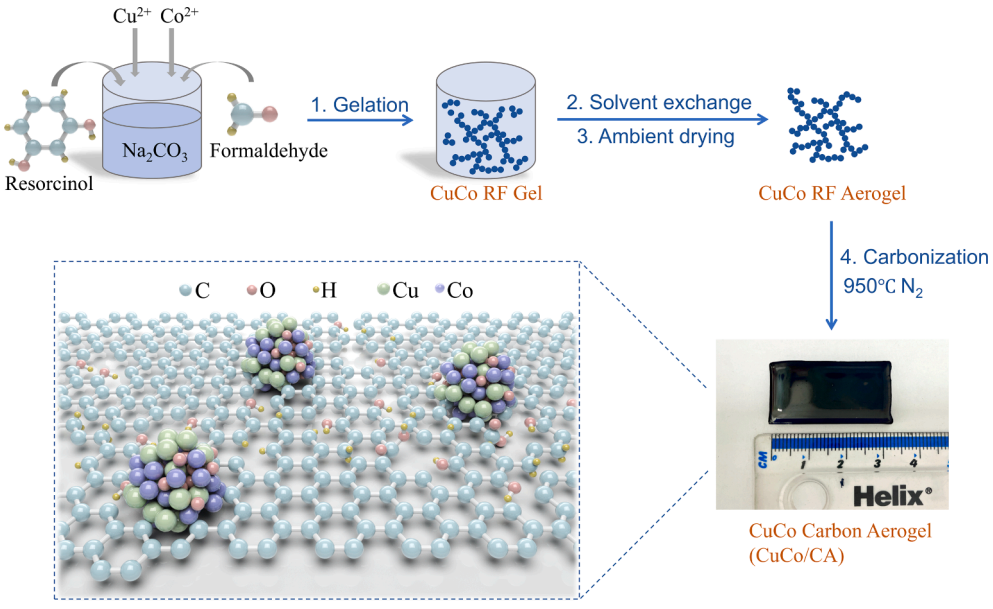

Fig. 1. Schematic diagram showing four-stage synthesis of CuCo/CA cathode. A similar process was utilised for the synthesis of Cu/CA, Co/CA and CA.

min prior to reaction to remove any oxygen. The initial pH of the solution was adjusted to the desired value using NaOH and H_2SO_4, and pH and dissolved oxygen (DO) concentration were monitored using a digital multi-meter kit (HQ 40d, Hach, UK). Water samples were withdrawn for measurement at preset intervals using a 10 mL syringe, followed by filtration through a 0.22 μ m filter. The cathode was collected and cleaned with ultra-pure water for the reuse experiments, where its recyclability was assessed based on the decomposition efficiency of TC.

The concentration of TC was measured using a UV–Vis spectroscopy (Shimadzu UV1900) at a detection wavelength of 357 nm [22]. The pseudo-first-order kinetic model was used to describe the removal of TC in Equation (4), where C_0 represents initial pollutant concentration (mg/L), C_t represents pollutant concentration at time t (mg/L), k_{obs} is apparent rate constant (min^{-1}) and t represents reaction time (min), respectively.

$$ln(C_0/C_t) = k_{obs}t \quad (4)$$

2.3. Continuous stirred tank reactor

The operational stability of the CuCo/CA cathode was also investigated using a continuous stirred tank reactor (CSTR) over a 48 h reaction time. The reactor comprised an undivided cylindrical-shaped glass cell, two peristaltic pumps (Watson Marlow 323S), a DC power supply, and containers for the stock feed solution and a post-reaction disposal solution. Two peristatic pumps were employed to ensure a steady flow of TC solution through the reactor. One pump was used to feed the stock solution into the reactor, and the other pump was used to collect the treated solution; the pumps were calibrated to maintain a steady reactor solution volume. The cell was equipped with a platinum sheet anode and CuCo/CA cathode with a 2 cm inter-electrode separation. A supporting electrolyte of 0.05 M Na_2SO_4 and a model contaminant solution of 10 mg/L TC were utilised. Continuous stirring of the sample solution was achieved using a magnetic stirrer and PTFE magnetic bar.

2.4. Characterization methods

X-ray diffraction (XRD) patterns were obtained using a Cu K Alpha radiation source (λ = 1.5406 Å) scanning in the 2θ range of 10° to 80° with a step size of 0.02° using a Shimadzu XRD-6100 instrument. The surface morphology information was obtained through high-resolution transmission electron microscopy (HRTEM) using a FEI Titan3 Themis 300 instrument. The energy dispersive X-ray spectroscopy (EDS) mapping was executed using the same instrument employed for HRTEM with a HAADF detector. X-ray photoelectron spectroscopy (XPS) was characterised using an ESCALAB XI^+ (Al Kα radiation) manufactured by Thermo Scientific was used to perform C1s, O1s, Cu2p and Co2p orbital spectrum scanning on the CuCo/CA sample to analyse the chemical state of the elements on the surface. Experimental Fourier Transform Infrared (FTIR) diffuse reflection spectra were recorded using a Nicolet iS5 (Thermo Scientific) on powder-pressed KBr pellets. Defects and disorder information of the cathodes were obtained using Raman microscopy (Horiba Scientific LabRAM HR Evolution) equipped with an excitation source at 514 nm (1.5 mW laser power, spot diameter of 2 μm). To investigate the surface porosity information of the synthesized cathodes, a Micromeritics Tristar 3000 instrument was used to obtain N_2 adsorption–desorption isotherms at a temperature of 77 K. Prior to conducting measurements, the samples underwent a vacuum degassing process at 393 K for 16 h to effectively eliminate any residual moisture. N_2 adsorption data acquired within the range of relative pressures from 0.05 to 0.16 kPa were selected to calculate the Brunauer-Emmet-Teller (BET) surface area. Furthermore, the assessment of pore size distributions was accomplished through the application of the Barrett-Joyner-Halenda (BJH) method [23] with data collected from the desorption branch.

2.5. Electrochemical properties tests

Cyclic voltammetry (CV) tests were carried out using a three-electrode system utilizing a CHI 760E electrochemical workstation (Chenhua Instrument Co.Ltd., China). To prepare the working electrode, the bulk CuCo/CA sample was first ground into powder. Subsequently, 10 mg of the powder was dispersed in a solvent comprising 1.5 mL of Milli-Q^{TM} water, 0.75 mL of ethanol, and 25 μL of 5 wt% Nafion solution. Following 1 h of sonication, the resulting catalyst ink (6 μL) was drop-cast onto a glassy carbon electrode surface (diameter: 3 mm) and left to air-dry naturally, forming a uniform catalyst film layer. The obtained electrodes were used as the working electrode, and platinum sheet and Ag/AgCl served as the counter and reference electrodes, respectively. The CV curve was recorded in O_2-saturated electrolyte (0.1 M Na_2SO_4 at pH = 5) with a scan rate of 10 mV/s. Before starting the test, the electrolyte was aerated with O_2 for 30 min to achieve saturation, and aeration was maintained at 0.3 L/min throughout the test.

Electrochemical impedance spectroscopy (EIS) measurements were performed employing a three-electrode system, in which the bulk synthesised samples served as the working electrode, and platinum sheet and Ag/AgCl functioned as the counter and reference electrodes, respectively. The EIS experiments were conducted using a potentiostat (Gamry, 1010E) across a frequency range of 10^{-2}-10^{-5} Hz with an amplitude of 5 mV.

Rotating ring-disk electrode (RRDE) testing was used to assess oxygen reduction reaction (ORR) activity and selectivity. RRDE voltammograms were recorded in 0.1 M Na_2SO_4 at pH 3 using an AFMSRCE rotator unit (Pine Instrument Company, United States). The preparation of catalyst ink was identical as for CV testing. 12 μL of the catalyst ink was pipetted and spread onto a glassy carbon disk electrode for the RRDE tests. The RRDE setup comprised of a GC disk (0.2475 cm^2) and a Pt ring (0.1866 cm^2) with a catalyst loading density of 213 μg/cm^2. Following overnight air-drying at room temperature, the modified RRDE was employed as the working electrode, equipped with an Ag/AgCl reference electrode and a platinum wire counter electrode. Prior to testing, the electrolyte was aerated with O_2 for 30 min. To eliminate the capacitive current of the working electrode, the background current was measured under an N_2 atmosphere using the same rotation speed (1600 rpm) and scan rate (10 mV/s) as those used under O_2, and then subtracted from the ORR polarization curve. The Pt ring electrode was held at a constant potential of 1.3 V vs. the reversible hydrogen electrode (RHE).

3. Results and discussion

3.1. Characterization and electrochemical performances

Physical and chemical characterisations are typically employed to gain insights into the catalytic mechanisms and performances. The crystalline composition of CuCo/CA cathode was first analysed through X-ray diffraction (XRD) (Fig. 2(a)). CuCo/CA exhibits a mixed phase comprising graphitic carbon, Co, Cu and Cu_2O. Three distinct diffraction peaks (44.2°, 51.5°, and 75.8°) corresponding to (1 1 1), (2 0 0), and (2 2 0) planes of Co indicated the incorporation of Co species into the carbon matrix [24]. The characteristic 2θ peak at ~ 23° is attributed to the crystallographic reflection of graphitic carbon [25]. Peaks at 2θ values of 36.4°, 42.3°, and 61.3° match the (1 1 1), (2 0 0) and (2 2 0) planes of Cu_2O [12], which might be beneficial to an overall enhancement of catalytic performance. Additionally, the peaks at 43.3°, 50.4° and 74.1° corresponding to Cu phase [26] confirmed the successful incorporation of elemental Cu into the carbon aerogel framework.

High-resolution transmission electron microscopy (HRTEM) images at various magnifications are shown in Fig. 2(b)—(d). They illustrate the uniform dispersion of metallic nanoparticles with a diameter of ~ 100 nm in CuCo/CA. These particles within the organic aerogel matrix promote the formation of graphite clusters during carbonization (Fig. 2

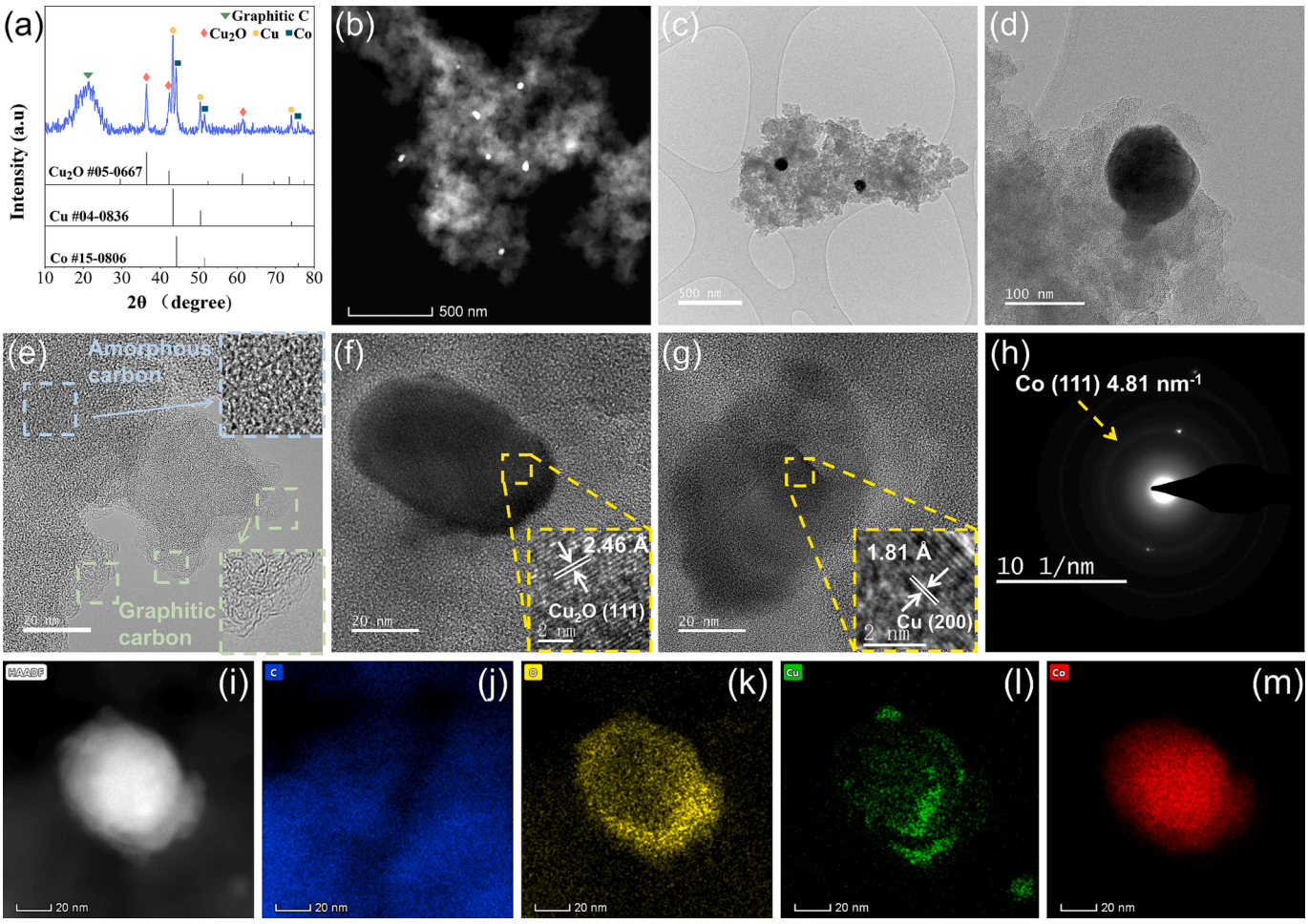

Fig. 2. (a) XRD patterns, (b)-(g) HRTEM images, (h) Electron diffraction pattern, and (i) HAADF-STEM images of CuCo/CA cathode; EDS mapping of (j) C, (k) O, (l) Cu and (m) Co element on CuCo/CA.

(e)). Notably, partial graphitization within carbon aerogel was previously reported when transition metals such as Fe, Ni and Co were used as doping metals, which endows the materials with good electrical conductivity and is conducive to efficient transport of electrons [27]. HRTEM images in Fig. 2(f)-(h) provide clear insight into interlayer distance and electron diffraction ring. Specifically, the measured spacing of 0.246 nm and 0.181 nm respectively corresponded to Cu_2O (1 1 1) and Cu (2 0 0) planes, and the electron diffraction ring is associated with Co (1 1 1) [28], in accordance with XRD findings. Furthermore, energy dispersive X-ray spectroscopy (EDS) mappings in Fig. 2(i)-(m) and Fig. S1 clearly show that elemental O is distributed in both carbon matrix and nanoparticles, while Cu and Co are selectively positioned in the central nanoparticle area. The distributions of elemental Cu and O on particles are correlated, with both being predominantly located at the edges of particle (see line scanning results), possibly due to the formation of Cu_2O. In contrast, elemental Co exhibits homogeneous distribution on the nanoparticle scale.

In a previous study by Lu et al., [29] a positive correlation was observed between oxygen content and both activity and selectivity in oxygen reduction reaction (ORR), thus indicating the significance of oxygen functional groups. Fig. 3(a) exhibits a Fourier-transform infrared spectroscopy (FTIR) obtained in investigation of oxygen-containing functional groups on the synthesized cathodes. Two obvious adsorption peaks at ~ 1407.8 cm^{-1} and ~ 1637.3 cm^{-1} are attributed to –COO- and −C=O bond stretches, respectively [30]. Additionally, strong adsorption peaks at 3444.2 cm^{-1} correspond to –OH vibration [31], which indicated the presence of abundant oxygen functional groups on synthesised CuCo/CA. By comparing the FTIR peak intensity between these four cathodes, the doping of Cu and Co elements on carbon aerogel is conducive to the formation of oxygen-containing functional groups, especially –COO- groups. The O 1 s high-resolution spectrum obtained from CuCo/CA using X-ray photoelectron spectroscopy (XPS) in Fig. 3 (b) is deconvoluted into the following bands: carboxyl bond (–COOH) at ~ 531.2 eV, oxygen doubly bound to carbon (C=O) at 532.1 eV, hydroxyl bond (–OH) at 533.0 eV, and oxygen singly bound to carbon (C–O–C) at 533.9 eV [32]. According to a previous study [33], the introduction of surface –COOH groups has a positive impact on the electrocatalytic process of $2e^-$ ORR for the generation of H_2O_2.

In addition to oxygen-containing functional groups, carbon defects are also regarded as active sites for catalytic two-electron ORR [29]. The defect degree of four cathodes were assessed through Raman spectroscopy in Fig. 3(c). Two prominent peaks are observed at ~ 1340 cm^{-1} (D band) and ~ 1583 cm^{-1} (G band), which represent disordered structure of sp^3 hybridised carbon atoms (suggesting defect degree) and aromatic ring structure of sp^2 hybridised carbon atoms (suggesting degree of graphitization), respectively [34]. By employing peak fitting analysis, I_D/I_G ratios calculated using the peak area are determined as: 1.88 (CuCo/CA), 1.55 (Cu/CA), 1.58 (Co/CA) and 1.65 (CA). These ratios signify that while synthesised cathodes possess abundant defect sites and structural distortions, they retain a considerable degree of graphitic structure. In comparison, the higher I_D/I_G value observed for CuCo/CA provide clear evidence that the synergistic effect of Cu and Co increases the number of carbon defects to improve ORR activity. A similar bimetallic effect has also been found in other carbon materials [11,35].

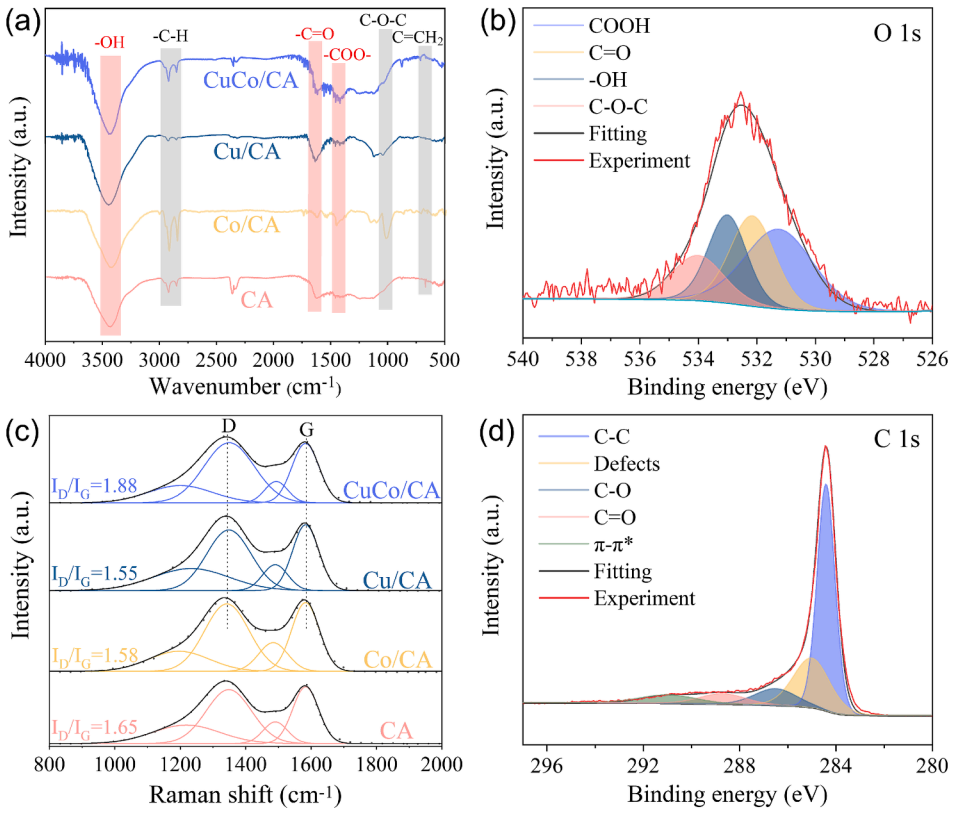

Fig. 3. (a) FTIR spectra of various cathodes; (b) O 1 s XPS spectra of CuCo/CA; (c) Raman spectra various cathodes and (d) C 1 s XPS spectra of CuCo/CA.

Furthermore, deconvolution of C 1 s spectrum (Fig. 3(d)) of CuCo/CA also shows a carbon defect peak at 285.4 eV [36], and the presence of C–O and C=O groups correspond to the O 1 s spectrum. These results indicated that a large number of carbon defects were formed during the carbonization process of CuCo/CA, promoting the generation of oxygen functional groups. These groups are considered to be catalytic sites for the two-electron ORR process [37], facilitating H_2O_2 generation.

The ORR electrocatalytic activity of CuCo/CA was directly evaluated using conventional three-electrode cyclic voltammetry (CV) in oxygen-saturated 0.1 M Na_2SO_4 (pH = 5) electrolyte solution. As illustrated in

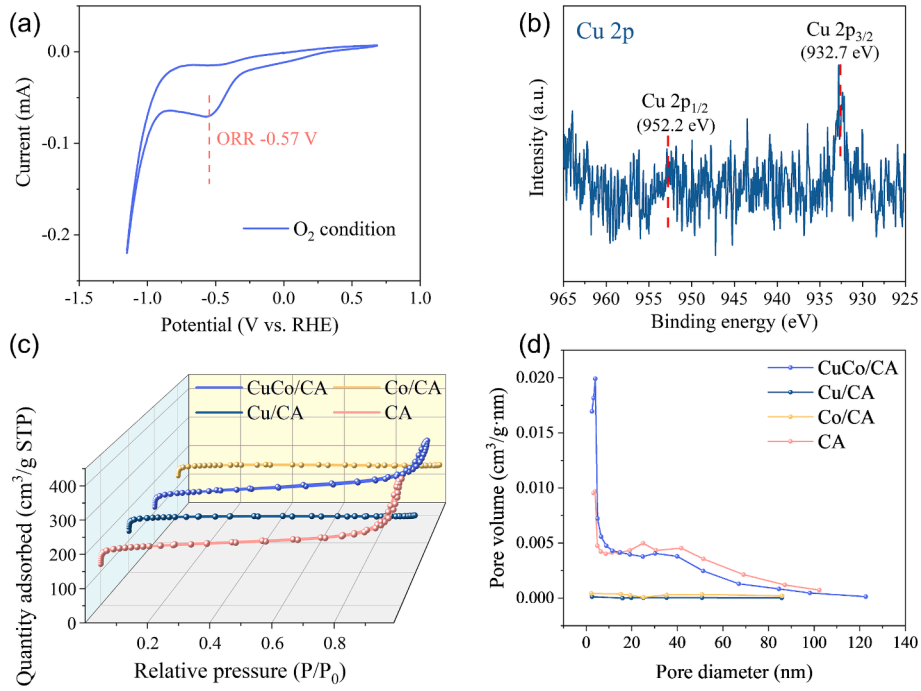

Fig. 4. (a) CV curve of CuCo/CA in the presence of O_2; (b) Cu 2p XPS spectrum of CuCo/CA; (c) N_2 adsorption–desorption isotherms and (d) Pore size distribution curves of various cathodes.

Fig. 4(a), a distinct peak at approximately −0.57 V vs. reversible hydrogen electrode (RHE) is observed due to the reduction of O_2, reflecting the catalytic activity of the CuCo/CA cathode for oxygen reduction [38]. The bulk metallic content of CuCo/CA was determined using inductively coupled plasma mass spectrometry (ICP-MS) with copper (Cu) and cobalt (Co) loadings at 1.00 wt% and 0.94 wt%, respectively (Table 1). Due to low metal loadings, elemental Cu and Co are not observed in the full XPS spectrum, whilst obvious signals for C and O are detected (Fig. S2(a)). In the high-resolution XPS spectrum of Cu 2p (Fig. 4(b)), two sub-peaks of Cu 2p 3/2 and Cu 2p 1/2 at 932.7 eV and 952.2 eV correspond to Cu(I) [39], further verifying the presence of Cu_2O in the CuCo/CA cathode and consistent with XRD results. Fig. S2 (b) shows the high-resolution XPS spectrum of Co 2p, and two peaks emerge at 780.1 eV and 795.5 eV, corresponding to Co 2p3/2 and Co 2p1/2 spin–orbit peaks, respectively [40]. According to a previous study [41], Cu(I) species are regarded as a Fenton-like catalyst and have been applied in H_2O_2 activation to generate ·OH radicals, as shown in Equation (3). Additionally, it has been widely reported that Co^{2+}/Co^{3+} redox couples play a crucial role in enhancing the Fenton-like reaction by facilitating the *in situ* activation of H_2O_2 to generate hydroxyl radicals ($Co^{2+} + H_2O_2 \rightarrow Co^{3+} + \bullet OH + OH^-$) [42–47]. The presence of catalytically active metal components thus endows CuCo/CA cathode with another important role as an integrated Fenton-like catalyst to induce radical generation.

Pore structure properties of the synthesised cathodes were analysed by N_2 adsorption–desorption tests as shown in Fig. 4(c)-(d), and Table 1. The synthesised cathodes possess a BET surface area of 574 ~ 601 m^2/g, surpassing some other reported carbon aerogels [48,49]. The relatively high specific surface area not only exposes abundant active sites on the surface but also imparts strong adsorption forces between cathodes and pollutant compounds. Pure CA exhibits the highest adsorption pore volume of 0.343 cm^3/g, it is therefore speculated that the porous characteristics mainly originate from the carbon skeleton, and the abundant nanoparticles occupy adsorption sites and pore channels.

Cu/CA and Co/CA curve (Fig. 4(c)) exhibits IUPAC Type I isotherm behaviour, with a rapid increase in gas adsorption capacity in relatively low-pressure region, which indicated a typical microporous structure [50]. Negligible adsorption pore capacity was observed for Cu/CA and Co/CA within the detected range of 2.6-157.9 nm, as shown in Fig. 4(d). This is because nitrogen, as the adsorbate gas, is limited by its molecular size, making it unable to easily penetrate extremely small pores. Consequently, micropores (smaller than 2 nm) cannot be accurately detected. The curves for pure CA and CuCo/CA exhibit an isotherm of IV featuring H3-type hysteresis loops, reflecting their prominent mesoporous structure [51]. These observations are consistent with narrow mesopore size distributions for CA and CuCo/CA, centered at 2.6 nm and 4.0 nm respectively. In addition, a rapid increase in gas adsorption within low relative pressure region is observed for both CA and CuCo/CA, indicating the coexistence of a micropore structure. Micropores provide a number of active sites for the process of oxygen reduction, whereas *meso*-macro pores serve as channels for oxygen transport, facilitating oxygen supply and allowing electrolyte to infiltrate the interior of the cathode. [52]. The combination of two roles greatly improves catalyst's oxygen reduction performance [53].

A previous investigation found that pore structures of electrode materials also had an effect on electrochemical performance [54]. Electrochemical impedance spectroscopy (EIS) Nyquist plots of four cathodes all exhibit an incomplete semicircle in the high-frequency range and a straight line in the low-frequency range (Fig. 5(a)). The charge transfer resistance (R_{ct}) of each cathode was qualitatively compared by analysing the radius of the semicircle in the Nyquist plots. The CuCo/CA electrode exhibited the smallest semicircle radius, indicating the lowest charge transfer resistance and enhanced electron transfer kinetics, while Cu/CA showed the largest semicircle radius, reflecting its relatively inferior electrochemical performance. These results suggest that the synergistic effect of Cu and Co resulted in a reduction of charge transfer resistance of carbon aerogel, indicating a more efficient electron transfer process between the electrode–electrolyte interface [55].

To further investigate the synergistic effect of Cu and Co on ORR activity and selectivity, a rotating ring-disk electrode was used to evaluate ORR performance at 1600 rpm. Fig. 5(b) shows oxygen reduction currents observed on the disk electrode and the corresponding H_2O_2 oxidation currents measured at 1.3 V on the ring electrode. Linear sweep voltammetry (LSV) outcome reveals that CuCo/CA and pure CA have very similar ORR performance, which may be due to their similar porosity characteristics. The ORR half-wave potential ($E_{1/2}$) of CuCo/CA, Cu/CA, Co/CA and pure CA were measured as 0.056 V, −0.265 V, 0.144 V and 0.047 V (vs. RHE), respectively. The results show that addition of Co to Cu/CA increased ORR activity, reflected by a 321 mV positive shift in the half-wave potential [56]. Co/CA exhibits the highest ORR activity due to the most positive half-wave potential; however, it has the lowest 2 e^- ORR selectivity due to the lowest ring current density tested. On the other hand, the incorporation of Cu enhances the selectivity for 2e^- ORR, as the ring current exhibits significant increases for CuCo/CA electrode compared to Co/CA. The enhanced ORR properties are attributed to the fact that the synergistic effect of Cu and Co enables carbon aerogel to form a unique microstructure during the synthesis process, with abundant carbon defects and oxygen functional groups. The synergistic effect of the two metals offsets the shortcomings of the single metal. Overall, CuCo/CA has outstanding performance in both ORR activity and selectivity, so it can catalyse the heterogeneous

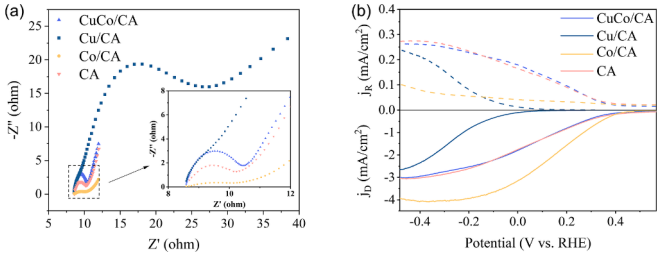

Fig. 5. (a) EIS Nyquist plots; (b) Polarisation curves of different electrodes at 1600 rpm and simultaneous H_2 O_2 oxidation currents at the ring electrode in 0.1 mol/L Na_2 SO_4 at pH = 3.

Table 1
Porosity and metal loadings of synthesized cathodes.

Electrode	BET surface area (m^2/g)	t-Plot micropore area (m^2/g)	t-Plot micropore volume (cm^3/g)	BJH adsorption cumulative volume (cm^3/g)	ICP [wt.%]	
					Cu	Co
CA	601.4	480.3	0.223	0.343	/	/
Cu/CA	583.8	531.5	0.248	0.009	0.93 ± 0.02	/
Co/CA	576.6	533.7	0.249	0.002		0.91 + 0.04
CuCo/CA	574.2	453.1	0.209	0.296	1.00 ± 0.03	0.94 ± 0.04

electro-Fenton system to potentially achieve the highest pollutant removal efficiency.

3.2. Hetero electro-Fenton performance

3.2.1. Degradation performance and radical generation

Utilising tetracycline (TC) as a candidate pollutant, enabled the performance of different heterogeneous electro-Fenton systems to be evaluated. As depicted in Fig. S3(a), pseudo-first-order kinetic plots for TC removal were observed for the synthesised cathodes under neutral pH conditions. The corresponding kinetic rate constant in the CuCo/CA EF system was 0.988 h^{-1}, which was 2.16, 2.06 and 2.21 times as fast as Cu/CA (0.457h^{-1}), Co/CA (0.481 h^{-1}) and pure CA (0.447 h^{-1}), respectively (Fig. S3(b)). The electro-sorption (ES) of these porous cathodes was further investigated at an operating current of 1 mA and under an N_2 atmosphere, where oxidative degradation could not contribute to TC removal. As shown in Fig. 6(a) (dashed lines), pure CA electrode (characterised by distinctive porous structure and highest surface area) exhibited the highest adsorption capability of 65%. In contrast, the ES capacity of CuCo/CA electrode almost reached 50% after 2.5 h, potentially due to its smaller specific surface area [57]. Notably, TC degradation employing CuCo/CA electrode increased significantly up to 93% (Fig. 6(a)-solid lines) after 2.5 h. This was indicative of high reactivity for both adsorption and oxidative degradation pathways in the CuCo/CA EF system. In comparison, TC removal rate with pure CA, Co/CA and Cu/CA in EF systems was 70%, 67% and 65%, respectively, which demonstrated TC removal using these cathodes was mainly ascribed to their high electro-sorption capacities. Since the synergistic effect of Cu and Co transition metals on carbon aerogel greatly enhances the catalytic performance, the impact of Cu/Co metal ratio was further investigated, as shown in Fig. S4. The $Cu_{0.5}Co_{0.5}$/CA electrode, with an optimal Cu/Co ratio of 1.0, achieved the highest TC removal efficiency of 90%. Within 150 min, the TC removal efficiencies for $Cu_{0.3}Co_{0.7}$/CA and $Cu_{0.7}Co_{0.3}$/CA electrodes were 60.6% and 68%, respectively.

Moreover, electricity consumptions and costs of EF processes based on CuCo/CA, Cu/CA, Co/CA and pure CA cathodes were evaluated according to Equation (5) [58].

$$EC_{TC}\left(kWh/kg_{TC}\right) = I \bullet V \bullet t/\Delta m_{TC} \quad (5)$$

where EC_{TC} (kWh/kg_{TC}) is electricity consumption per kg TC degradation, I is current (A), V is average voltage (V), t is reaction time (h), Δm_{TC} is TC mass loss (g). The average commercial electricity price in the UK is £0.27 /kWh in 2024 [59]. As shown in Table 2, the CuCo/CA-based EF system demonstrates exceptional electrocatalytic efficiency for TC degradation, achieving the least electricity consumption. Importantly, the energy consumption for degrading each kilogram of TC in the CuCo/CA EF system requires only approximately one-fifth of that for previously reported electro-Fenton systems [60], indicating the practical application potential of this process.

To further elucidate reactive species involved in the oxidative degradation of TC in a CuCo/CA EF system, *tert*-butanol (TBA) was used as a ·OH radical scavenger. TBA was chosen because of its high rate constant with ·OH radical ($k = 6.0 \times 10^8$ $M^{-1}s^{-1}$) [61]. The results in Fig. 6(b) show that the TC degradation rate gradually decreased with increasing TBA dosage. The reaction rate constant decreased from 0.847 h^{-1} to 0.364 h^{-1} with the addition of 1 M TBA into the system (Fig. S5), demonstrating the key role of ·OH radicals in the oxidative degradation of TC. P-Benzoquinone (p-BQ) has also been used as a $\cdot O_2^-$ radical scavenger with a high rate constant with $\cdot O_2^-$ ($k = 0.9–1.0 \times 10^9$ $M^{-1}s^{-1}$) [62]. Our results showed that addition of p-BQ led to a drop in TC degradation rate from 87% to 65%. These results suggest that O_2 initially undergoes reduction to an $\cdot O_2^-$ radical intermediate *via* a one-electron pathway, which is then followed by further reduction to H_2O_2, and subsequently ·OH [49]. Furthermore, electron spin resonance (ESR) spectroscopy was used with DMPO as a spin-trapping agent to directly prove the generation of ·OH and $\cdot O_2^-$ radicals in the CuCo/CA EF process. As shown in Fig. 6(c), the characteristic peak with intensity

Table 2
Electricity consumption and cost. Conditions: pH_0 -7.0, Na_2SO_4 -50 mM, TC-10 mg/L, 20 mA.

EF system	I (A)	$V_{average}$ (V)	t (h)	Δm_{TC} (g)	EC_{TC} (kWh/kg_{TC})	Electricity cost (£/kg_{TC})
CuCo-CA	0.02	2.375	2.5	1.3875×10^{-3}	85.59	23.11
Cu-CA	0.02	2.642	2.5	0.981×10^{-3}	134.66	36.36
Co-CA	0.02	2.471	2.5	1.005×10^{-3}	122.94	33.19
CA	0.02	2.495	2.5	1.0425×10^{-3}	119.66	32.31

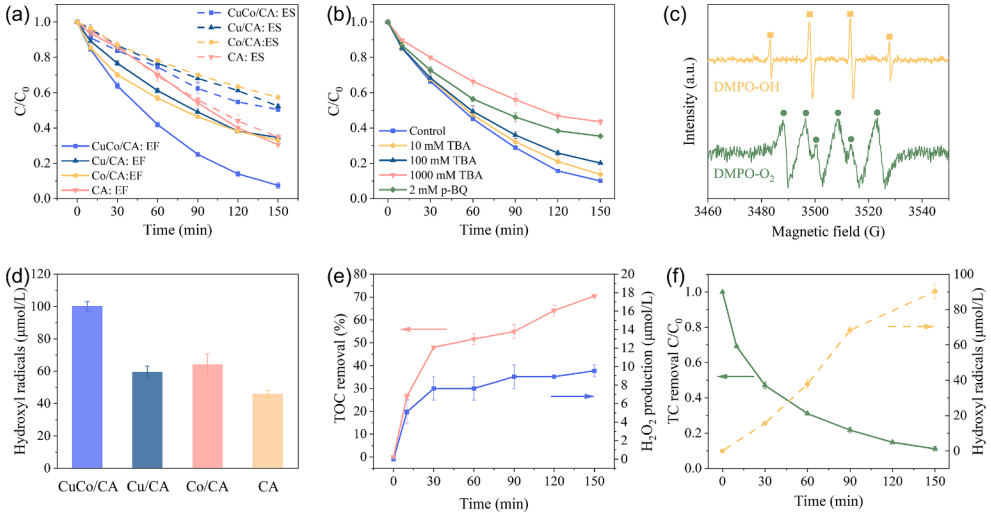

Fig. 6. (a) TC removal in electro-sorption (ES) and electro-Fenton (EF) systems; (b) Effect of radical scavengers on TC degradation in CuCo/CA EF system; (c) ESR spectra for CuCo/CA EF system; (d) Production of hydroxyl radical after 150 min; (e) TOC removal (left) and H_2 O_2 production (right) in CuCo/CA EF system. Conditions: pH_0 7.0, Na_2 SO_4 50 mM, TC 10 mg/L, salicylic acid 0.01 M, no external aeration and 20 mA for EF systems, 0.2 L/min N_2 and 1 mA for ES systems. (f) TC removal (left) and hydroxyl radical generation (right) in the presence of CuCo/CA powder (0.2 g/L) and externally supplied H_2 O_2 (50 ppm).

ratio of 1:2:2:1 corresponding to DMPO-·OH adduct was observed in a EF system utilising CuCo/CA as the cathode, thereby confirming the generation of ·OH species [41]. The sextuplet ESR signal of DMPO-·O_2^- spin adduct was also detected [63], which is consistent with the results of quenching experiments. The effective degradation of TC in CuCo/CA EF system was primarily induced by an indirect oxidation process in the presence of O_2, which is dominated by ·OH species. Under the attack of ·OH radicals, a total organic carbon (TOC) removal efficiency of 70.46% after 2.5 h was achieved under optimal operating conditions (Fig. 6(e), left axis), demonstrating the system's ability to effectively break down the pollutants into mineralised products.

The concentration of electro-generated ·OH was also quantified using the probe reaction of salicylic acid and ·OH [64]. As shown in Fig. 6(d), the accumulated concentration of ·OH in CuCo/CA EF system was determined to be 100.1 μ mol/L after 150 min without external aeration. In comparison, the production of ·OH in EF systems using Cu/CA, Co/CA and pure CA cathode reached 59.3 μ mol/L, 63.9 μ mol/L and 45.9 μ mol/L, respectively. This result further indicates that the removal of TC with Cu/CA, Co/CA and pure CA is mainly through electro-sorption processes. Table S1 summarises ·OH production rate in various electro-Fenton systems [65–71], showing that the CuCo/CA based EF system has a stronger ability to generate ·OH radicals than these previously reported EF systems, indicating that the proposed system has great application prospects in oxidative degradation of organic contaminants.

Previous studies have indicated that H_2O_2 can be electro-generated *via* two-electron ORR pathways on carbon-based materials [72]. However, the concentration of accumulated H_2O_2 over CuCo/CA was negligible, measured at 8.9 μm ol/L within 2 h (Fig. 6(e), right axis). Such an observation may be attributed to its rapid on-site decomposition into reactive ·OH intermediates [48]. Additionally, in an undivided electro-Fenton system, the generated H_2O_2 can undergo chemical or electrochemical decomposition via disproportionation ($H_2O_2 \rightarrow H_2O + 1/2O_2$) and reduction at the cathode ($H_2O_2 + 2e^- \rightarrow 2OH^-$) [73]. The plateau indicates that a steady-state balance is reached between H_2O_2 generation and its consumption or decomposition, which highlighted the system's efficiency in maintaining active hydroxyl radical generation for pollutant degradation. Similar research findings also suggest that alloy particles encapsulated within carbon matrix enable modulation of local electronic environment, facilitating the activation of H_2O_2 via a $1e^-$ pathway to generate OH radicals [74]. To investigate whether CuCo/CA participated in the activation process of H_2O_2, TC degradation and ·OH generation efficiency were measured in a system comprised of CuCo/CA powder and externally added H_2O_2. Fig. 6(f) shows that TC removal reached 89% and 90 μ mol/L of ·OH radical was generated at 150 min reaction time, in the presence of 50 ppm H_2O_2 and 0.2 g/L CuCo/CA nanoparticles. Hence, it could be inferred that the CuCo/CA cathode can not only induce $2e^-$ electrochemical process of oxygen reduction to produce H_2O_2, but also catalyse *in situ* activation of H_2O_2 to generate ·OH species further leading to TC degradation.

3.2.2. Optimization of operational conditions

In addition to inherent characteristics of the electrode, reaction conditions such as current density, pH value and aeration rate play a crucial role in the degradation efficiency of contaminants in EF systems. Fig. 7(a) shows that the increase in current density accelerated electron transfer rate in ORR process, however, excessive current and cathode potential led to side reactions such as hydrogen evolution ($2H^+ + 2e^- \rightarrow H_2$) and four-electron reduction of oxygen as shown in Equation (6) [75]. Within 150 min, TC removal reached its highest level of 90% at a current of 20 mA. However, continuing to increase current to 30 mA and 40 mA led to a reduction in TC degradation, dropping to 82% and 74%, respectively. This change might be due to occurrence of side reactions utilising part of the electrical energy. Acidic pH conditions, especially pH of 3, were more conducive to TC degradation in the CuCo/CA EF system (Fig. 7(b)). This is because the generation of H_2O_2 and ·OH required participation of H^+, as depicted in Equations (1) and (7), respectively. The highest first-order reaction rate constant of 1.08 h^{-1} was obtained under pH 3 condition, while TC degradation still reached 82%, 88% and 86% under pH conditions of 5, 7 and 9, respectively.

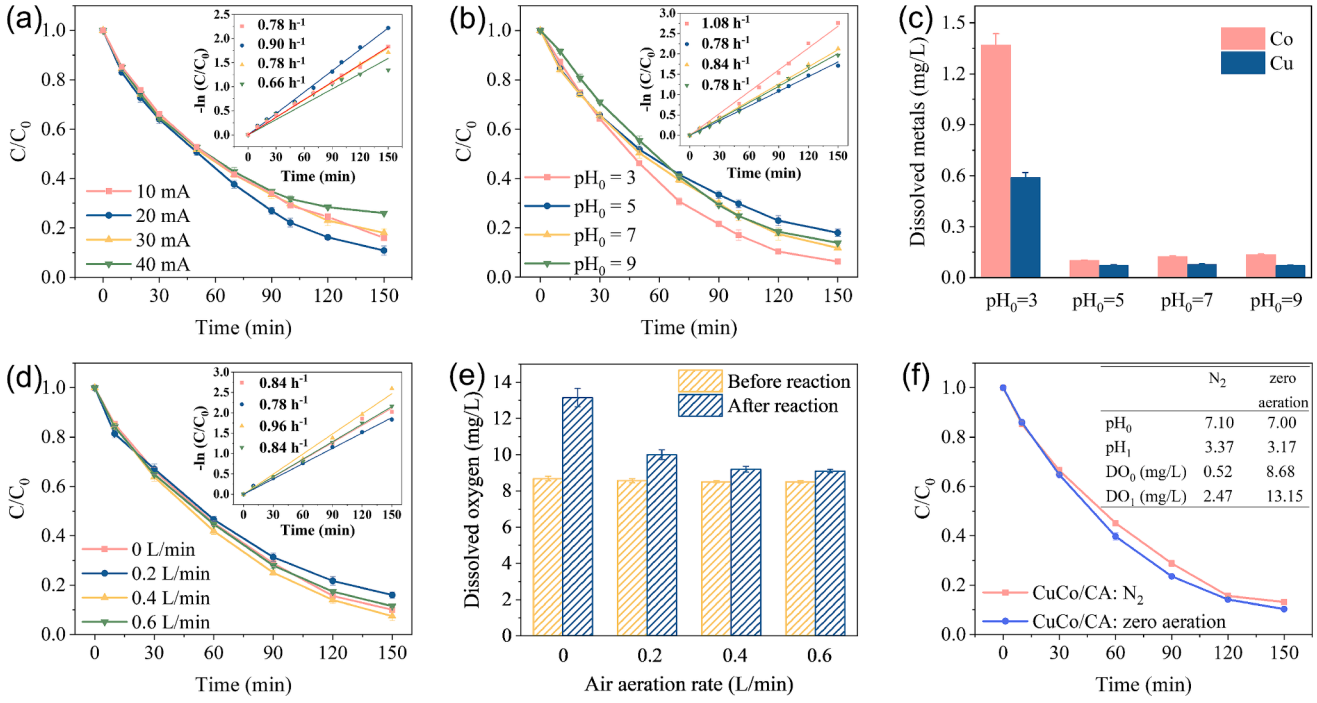

Fig. 7. Impact of (a) current (the corresponding voltage ranges are: 10 mA: 1.65–2.30 V, 20 mA: 2.00–2.75 V, 30 mA: 2.42–3.02 V, 40 mA: 2.74–3.51 V) and (b) initial pH in CuCo/CA EF system; (c) Metal leaching after 2.5 h reaction in CuCo/CA EF system; (d) Impact of airflow rate in CuCo/CA EF system; (e) Concentration of dissolved oxygen in CuCo/CA EF system; (f) Degradation of TC under an N_2 atmosphere and zero aeration. Inserted graphs are pseudo-first-order kinetic models with rate constants. Conditions: Na_2SO_4 = 50 mM, ACT = 10 mg/L, 200 mL/min N_2 for N_2 experiment.

These results demonstrated that the electro-Fenton system with CuCo/CA cathode has good adaptability to a wide range of pH conditions.

Furthermore, the amount of leached copper ions and cobalt ions at various pH values were recorded in Fig. 7(c), as well as further information in Fig. S6. Although strong acidic condition (pH 3) did lead to a notable release of Co ions initially, assessed as 1.37 ppm after 2.5 h reaction, results in Fig. S7 indicated that dissolution of metal ions significantly reduced in the second and third rounds of recycling runs. In the third run, leaching of Co and Cu ions after 150 min reaction time reduced to 0.21 ppm and 0.26 ppm, respectively. Under other pH conditions (such as pH 5, 7 and 9), dissolution of metal ions was also negligible whilst achieving considerable degradation performance (Fig. 7(c)).

$$O_2 + 2H_2O + 4e^- \rightarrow 4OH^- E^0 = 1.23V\ vs.RHE \quad (6)$$

$$H_2O_2 + e^- + H^+ \rightarrow \bullet OH + H_2O \quad (7)$$

The impact of airflow rate on TC removal efficiency was further examined and found to be negligible (Fig. 7(d)). The observed rate constants (inset) at airflow rates of 0, 0.2, 0.4 and 0.6 L/min were measured as 0.84, 0.78, 0.96 and 0.84 h^{-1}, respectively. The results indicated that TC can be effectively eliminated even without external aeration, achieving approximately 90% decomposition within 2.5 h reaction time. The dissolved oxygen (DO) was measured before and after treatment under various air flow rates, as shown in Fig. 7(e). Interestingly, following EF reaction, DO concentration in the system without external aeration increased from 8.68 mg/L to 13.15 mg/L, while pH decreased from 7.0 to 3.17 (Fig. 7(f)). As shown by Equation (8) [76], oxygen evolution reaction (OER) occurring near the anode could provide sufficient oxygen for the non-aerated system to complete electro-Fenton process, which led to efficient degradation of TC even without external aeration. Similar oxygen generation mechanisms from OER anode, even in the absence of aeration, have been reported in other electrochemical systems as well [77]. In addition, continuously generated H^+ ions caused a drop in pH value; the pH dropped from 7.0 to 3.2 after 2.5 h reaction time and remained more or less stable at around 3.2 (see Fig. S8). The subsequent formation of H_2O_2 and ·OH radicals *via* $2e^-$ and $1e^-$ reduction pathways required the involvement of H^+ ions. Consequently, maintaining a constant H^+ ion concentration was conducive to the generation of H_2O_2 and ·OH radicals.

$$2H_2O \rightarrow 4e^- + 4H^+ + O_2 \quad (8)$$

In order to investigate OER activity and oxygen transfer efficiency at the solid–liquid interface i.e., between electrolyte and electrode, a heterogeneous electro-Fenton TC degradation experiment was carried out under a nitrogen (N_2) atmosphere. The reactor was aerated with N_2 for 20 min to strip out as much dissolved oxygen as possible. DO concentration before reaction (DO_0) was 0.52 mg/L and increased to 2.47 mg/L after reaction (DO_1), while the solution pH decreased from 7.10 to 3.37 (Fig. 7(f)), demonstrating that OER still occurred under an N_2 atmosphere. This system was still able to achieve similar TC degradation to the zero-aeration system, which was around 90% removal after 150 min reaction time. These results indicate that once O_2 is generated near the anode it may be transferred through the solution and, at the solid–liquid interface, undergo a reduction process at the cathode even at low DO levels. The CuCo/CA cathode, characterised by its substantial surface area and pore volumes, facilitated the adsorption, storage and mass transfer of dissolved O_2, thus promoting efficient utilization of O_2 and electro-generation of H_2O_2 [78]. As a result, the oxygen produced at the anode proved adequate for sustaining H_2O_2 generation without the need for external aeration. This approach may be more cost-effective in comparison with previous electrochemical H_2O_2 generation methods requiring external aeration [4,64,79,80].

In summary, the synergistic effect of Cu and Co within CuCo/CA EF system can be ascribed to following aspects: (1) Structural improvements CuCo/CA features a large surface area and a structure with coexistence of micropores and mesopores, offering a number of active sites to promote more efficient interactions with contaminant molecules and leading to improved oxygen reduction reaction. The mesopores also function as gas transport channels, enhancing oxygen transport and promoting electrolyte penetration into the carbon matrix. (2) Enhanced electrocatalytic activity. Cu and Co are embedded in carbon aerogel, catalysing the graphitisation process of carbon matrix and leading to faster electron transfer. Furthermore, the introduction of CuCo alloy induces formation of carbon defects, which modify electronic structure and greatly boost its electrocatalytic performance. (3) Enhanced selectivity and activity of oxygen reduction. Presence of graphitic carbon promotes the generation of oxygen-containing group, which aid in oxygen reduction process. Moreover, the co-existence of Cu and Co results in lattice distortion and electronic environment adjustment that further enhance both selectivity and activity.

Based on above findings, the mechanisms for oxygen species production and TC degradation are illustrated in Fig. 8. Initially, oxygen evolution and accumulation take place near the anode, which are induced by an electric current effect. The produced oxygen subsequently diffuses to interface of electrolyte and cathode, where it goes through a $2e^-$ reduction pathway to produce H_2O_2. The excellent pore structure of CuCo/CA electrode achieves efficient oxygen transport and utilisation and eliminates the need for additional oxygen input to produce H_2O_2. Moreover, H^+ ions produced through oxygen evolution process establish an advantageous pH condition for $2e^-$ oxygen reduction and *in situ* H_2O_2 activation. Catalytically active Cu^+ and Co^{2+} on CuCo/CA cathode catalyse H_2O_2 activation on-site to produce highly oxidative ·OH radicals, thus enabling oxidative degradation of organic contaminants in water. Then, Cu^{2+} and Co^{3+} can subsequently be reduced back to Cu^+ and Co^{2+} at the cathode, completing the redox cycle. This cycle promotes continuous activation of H_2O_2 and enhances the overall efficiency of the electro-Fenton system.

3.3. Recyclability, stability, and broad applicability of CuCo/CA

In order to evaluate recyclability of the CuCo/CA cathode, six consecutive electro-Fenton TC degradation experiments were conducted. The results are shown in Fig. 9(a), in which the overall difference in TC degradation rates was very small. After six runs, the CuCo/CA electro-Fenton system achieved 84% TC removal within 150 min with a slight drop in the reaction rate constant (see Fig. S9). These results suggest that CuCo/CA, as an integrated electrode, could maintain stability during electro-Fenton process and retain good performance. The stability of the CuCo/CA cathode was further investigated in Fig. 9(b) using a continuous stirred tank reactor (CSTR, Fig. 9(c)) for a 48 h experiment under different flow velocities and initial TC concentrations. The results show that the CuCo/CA EF system with a slower flow rate and a lower TC concentration achieved higher removal performance due to longer hydraulic retention time. The electrocatalytic performance of CuCo/CA in all three systems was relatively stable over 48 h reaction time, despite a slightly reduced TC removal rate towards the end. This consistency in performance may due to the corrosion-resistant property of carbon-based aerogel material, with bimetallic particles well protected by outer carbon [49].

Further, the broad applicability of the CuCo/CA cathode was evaluated by investigating its degradation efficiency with various organic contaminants including antibiotics, analgesic, organic acid, and dye. Results in Fig. 9(d) and Fig. S10(a) show that the removal rates of tetracycline (TC), acetaminophen (ACT), metronidazole (MNZ), salicylic acid (SA) and acid orange 7 (AO7) were 90%, 94%, 93%, 84% and 95%, respectively, after 2.5 h reaction time. Pseudo-first-order plots were observed for all contaminant removal experiments, shown in Fig. S10 (b). The CuCo/CA EF system exhibited the highest apparent rate constant for MNZ removal, which was 1.12 h^{-1} (Fig. S10(c)). This performance highlights the relatively wide applicability of CuCo/CA

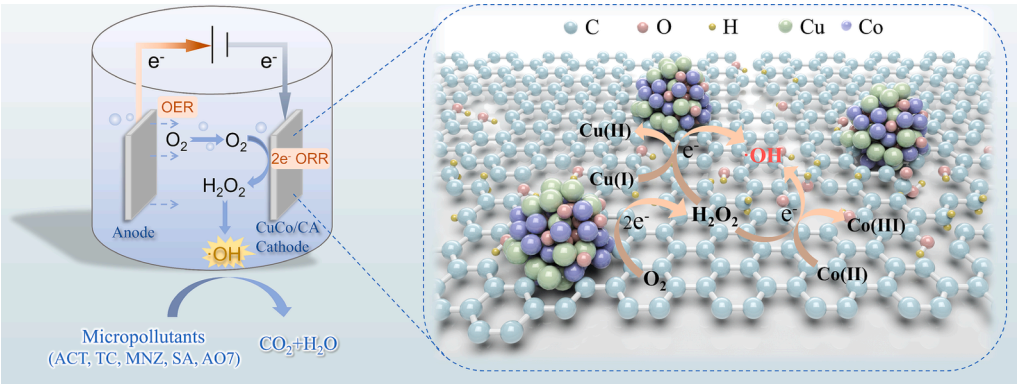

Fig. 8. Schematic of mechanisms for radical generation in CuCo/CA EF system.

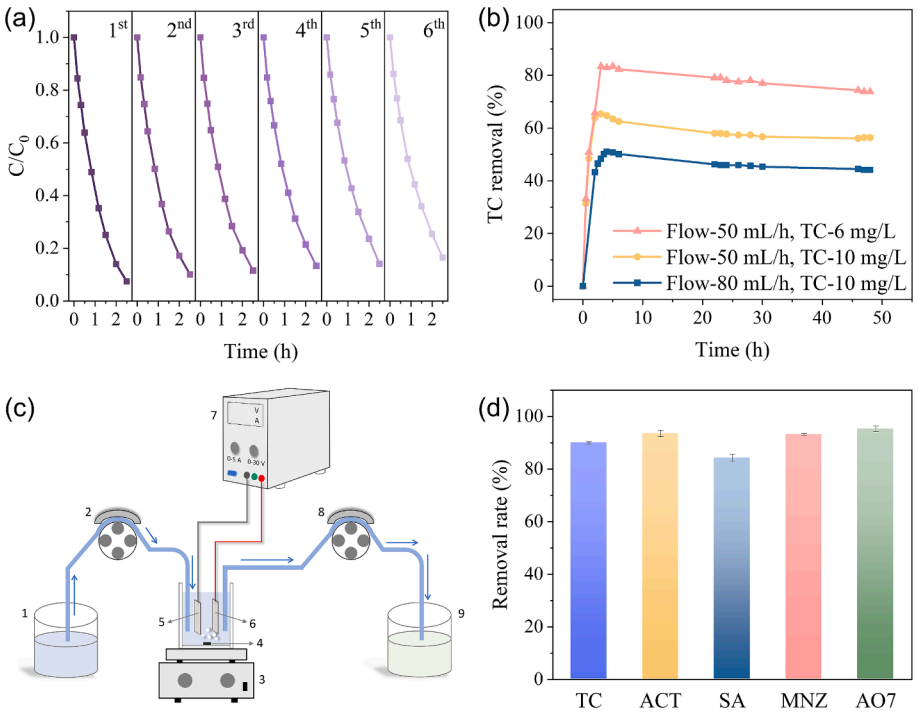

Fig. 9. (a) TC degradation in 6 consecutive CuCo/CA EF system runs; (b) TC removal during 48 h continuous stirred CuCo/CA EF system runs at varying fluid flow velocity; (c) Schematic diagram of the continuously stirred electro-Fenton reaction system: 1- Feed TC stock solution, 2 and 8 peristaltic pump, 3 – magnetic stirrer, 4 – PTFE stirrer bar, 5 – CuCo/CA cathode, 6 – platinum anode, 7 – DC power supply, 9 – post-reactor flow; and (d) The removal rate of various micropollutants in CuCo/CA EF system after 150 min. Conditions: pollutant = 10 mg/L, Na_2SO_4 = 50 mM, pH_0 = 7.0, 20 mA, zero aeration.

electrodes in a EF system for oxidative decomposition of various organic pollutants in water.

The above results indicate that CuCo/CA not only possessed high oxygen reduction catalytic activity but also exhibited long-term stability and recyclability. It demonstrates the desired removal efficiency for various organic pollutants, suggesting significant practical applications for water environmental remediation.

4. Conclusion

In this study, we have reported a novel electro-Fenton approach for selective 2e⁻ ORR and activation of *in situ* generated H_2O_2 using an integrated CuCo/CA cathode. The integration of Cu and Co into the carbon matrix enhanced the electro-generation of H_2O_2, conductivity, mass transfer, and oxygen reduction activity. The oxygen evolution process around the Pt anode provided advantageous pH conditions and oxygen supply for H_2O_2 production and radical generation near the cathode. As catalytically active metal components, Cu(I) and Co(II) imparted an additional role to CuCo/CA as an integrated catalyst inducing on-site H_2O_2 activation to form reactive ·OH species. Consequently, the established heterogeneous EF system exhibited promising TC removal (94%) within 2.5 h at pH 7 and a current density of 4.4 mA/cm^2. The High efficiency of CuCo/CA cathode in utilising oxygen eliminated the need for external aeration, which has greater industrial applicability compared to previously reported EF systems that require external aeration. The efficient degradation of TC primarily occurred through an indirect oxidation process dominated by ·OH radical. Importantly, ideal degradation efficiencies have been achieved over a wide pH range of 3–9, and CuCo/CA demonstrated good recyclability after six runs, and long-term stability after 48 h for continuous TC removal. Finally, the proposed technology exhibited high electrocatalytic activity towards various micropollutants. This research therefore offers an eco-friendly and sustainable approach to degrading persistent organic contaminants, presenting potential for advancing water decontamination

technologies.

CRediT authorship contribution statement

Qian Ye: Writing – original draft, Visualization, Investigation, Formal analysis, Conceptualization. **Timothy N. Hunter:** Writing – review & editing, Supervision, Resources, Methodology, Conceptualization. **Hao Xu:** Writing – review & editing, Methodology. **David Harbottle:** Writing – review & editing, Resources. **Girish M. Kale:** Writing – review & editing, Resources. **Martin R. Tillotson:** Writing – review & editing, Supervision, Resources, Methodology, Conceptualization.

Declaration of competing interest

The authors declare that they have no known competing financial interests or personal relationships that could have appeared to influence the work reported in this paper.

Acknowledgements

Qian Ye is funded by the China Scholarship Council (CSC, 202106240065) from the Ministry of Education of P.R. China. The authors are grateful to the funders and acknowledge their support of this work. The authors wish to express their gratitude to colleagues at the University of Leeds for their invaluable assistance: Dr. Jeanine Williams (HPLC), Ms. Karine Alves Thorne (metal loading analysis), and Dr. Ben Douglas (BET measurement). Special thanks are also due to Dr. David Elliott, Mr. Morgan McGowan, and Ms. Emma Tidswell for their guidance on laboratory equipment and technical support.

Appendix A. Supplementary data

Supplementary data to this article can be found online at https://doi.org/10.1016/j.seppur.2025.131597.

Data availability

The data associated with this paper is available from the University of Leeds White Rose Repository at https://doi.org/10.5518/1631.

References

[1] A.K. Sarmah, M.T. Meyer, A.B.A. Boxall, A global perspective on the use, sales, exposure pathways, occurrence, fate and effects of veterinary antibiotics (VAs) in the environment, Chemosphere 65 (2006) 725–759, https://doi.org/10.1016/j.chemosphere.2006.03.026.

[2] D. Qiao, Z. Li, J. Duan, X. He, Adsorption and photocatalytic degradation mechanism of magnetic graphene oxide/ZnO nanocomposites for tetracycline contaminants, Chem. Eng. J. 400 (2020) 125952, https://doi.org/10.1016/j.cej.2020.125952.

[3] M. Zhang, Y.-S. Liu, J.-L. Zhao, W.-R. Liu, L.-Y. He, J.-N. Zhang, J. Chen, L.-K. He, Q.-Q. Zhang, G.-G. Ying, Occurrence, fate and mass loadings of antibiotics in two swine wastewater treatment systems, Sci. Total Environ. 639 (2018) 1421–1431, https://doi.org/10.1016/j.scitotenv.2018.05.230.

[4] P. Dong, X. Chen, M. Guo, Z. Wu, H. Wang, F. Lin, J. Zhang, S. Wang, C. Zhao, H. Sun, Heterogeneous electro-Fenton catalysis with self-supporting CFP@MnO2-Fe3O4/C cathode for shale gas fracturing flowback wastewater, J. Hazard. Mater. 412 (2021) 125208, https://doi.org/10.1016/j.jhazmat.2021.125208.

[5] F. Sopaj, N. Oturan, J. Pinson, F. Podvorica, M.A. Oturan, Effect of the anode materials on the efficiency of the electro-Fenton process for the mineralization of the antibiotic sulfamethazine, Appl Catal B 199 (2016) 331–341, https://doi.org/10.1016/j.apcatb.2016.06.035.

[6] E. Mousset, L. Frunzo, G. Esposito, E.D. van Hullebusch, N. Oturan, M.A. Oturan, A complete phenol oxidation pathway obtained during electro-Fenton treatment and validated by a kinetic model study, Appl Catal B 180 (2016) 189–198, https://doi.org/10.1016/j.apcatb.2015.06.014.

[7] Y. Zhu, F. Deng, S. Qiu, F. Ma, Y. Zheng, L. Gao, A self-sufficient electro-Fenton system with enhanced oxygen transfer for decontamination of pharmaceutical wastewater, Chem. Eng. J. 429 (2022) 132176, https://doi.org/10.1016/j.cej.2021.132176.

[8] L. Cui, H. Huang, P. Ding, S. Zhu, W. Jing, X. Gu, Cogeneration of H2O2 and OH via a novel Fe3O4/MWCNTs composite cathode in a dual-compartment electro-Fenton membrane reactor, Sep. Purif. Technol. 237 (2020) 116380, https://doi.org/10.1016/j.seppur.2019.116380.

[9] P. Cao, X. Quan, K. Zhao, S. Chen, H. Yu, Y. Su, High-efficiency electrocatalysis of molecular oxygen toward hydroxyl radicals enabled by an atomically dispersed iron catalyst, Environ. Sci. Technol. 54 (2020) 12662–12672, https://doi.org/10.1021/acs.est.0c03614.

[10] K. Liu, J.-C.-C. Yu, H. Dong, J.C.S. Wu, M.R. Hoffmann, Degradation and mineralization of carbamazepine using an electro-Fenton reaction catalyzed by magnetite nanoparticles fixed on an electrocatalytic carbon fiber textile cathode, Environ. Sci. Technol. 52 (2018) 12667–12674, https://doi.org/10.1021/acs.est.8b03916.

[11] L. Cui, Z. Li, Q. Li, M. Chen, W. Jing, X. Gu, Cu/CuFe2O4 integrated graphite felt as a stable bifunctional cathode for high-performance heterogeneous electro-Fenton oxidation, Chem. Eng. J. 420 (2021) 127666, https://doi.org/10.1016/j.cej.2020.127666.

[12] C. Jin, Y. Cui, G. Zhang, W. Luo, Y. Liu, Y. Sun, Z. Tian, W. Zheng, Synthesis of copper-cobalt hybrid oxide microflowers as electrode material for supercapacitors, Chem. Eng. J. 343 (2018) 331–339, https://doi.org/10.1016/j.cej.2018.02.117.

[13] M. Huo, B. Wang, C. Zhang, S. Ding, H. Yuan, Z. Liang, J. Qi, M. Chen, Y. Xu, W. Zhang, H. Zheng, R. Cao, 2D metal–organic framework derived CuCo Alloy nanoparticles encapsulated by nitrogen-doped carbonaceous nanoleaves for efficient bifunctional oxygen electrocatalyst and zinc–air batteries, Chemistry – A European Journal 25 (2019) 12780–12788, https://doi.org/10.1002/chem.201902389.

[14] X. Feng, X. Yin, X. Bo, L. Guo, An ultrasensitive luteolin sensor based on MOFs derived CuCo coated nitrogen-doped porous carbon polyhedron, Sens. Actuators B 281 (2019) 730–738, https://doi.org/10.1016/j.snb.2018.11.010.

[15] Y. Liu, Z. Yang, J. Wang, Fenton-like degradation of sulfamethoxazole in Cu0/Zn0-air system over a broad pH range: performance, kinetics and mechanism, Chem. Eng. J. 403 (2021) 126320, https://doi.org/10.1016/j.cej.2020.126320.

[16] Y. Zou, H. Qi, Z. Sun, In-situ catalytic degradation of sulfamethoxazole with efficient CuCo–O@CNTs/NF cathode in a neutral electro-Fenton-like system, Chemosphere 296 (2022) 134072, https://doi.org/10.1016/j.chemosphere.2022.134072.

[17] H. Afanga, H. Zazou, F.E. Titchou, J.E. Gaayda, F. Sopaj, R.A. Akbour, M. Hamdani, Electrochemical oxidation of Naphthol Blue Black with different supporting electrolytes using a BDD /carbon felt cell, J. Environ. Chem. Eng. 9 (2021) 104498, https://doi.org/10.1016/j.jece.2020.104498.

[18] G. Gan, X. Li, S. Fan, L. Wang, M. Qin, Z. Yin, G. Chen, Carbon aerogels for environmental clean-up, Eur. J. Inorg. Chem. 2019 (2019) 3126–3141, https://doi.org/10.1002/ejic.201801512.

[19] D. Li, T. Zheng, Y. Liu, D. Hou, K.K. Yao, W. Zhang, H. Song, H. He, W. Shi, L. Wang, J. Ma, A novel Electro-Fenton process characterized by aeration from inside a graphite felt electrode with enhanced electrogeneration of H2O2 and cycle of Fe3+/Fe2+, J. Hazard. Mater. 396 (2020) 122591 https://doi.org/10.1016/j.jhazmat.2020.122591.

[20] H. Zhao, L. Qian, Y. Chen, Q. Wang, G. Zhao, Selective catalytic two-electron O2 reduction for onsite efficient oxidation reaction in heterogeneous electro-Fenton process, Chem. Eng. J. 332 (2018) 486–498, https://doi.org/10.1016/j.cej.2017.09.093.

[21] Q. Ye, T.N. Hunter, H. Xu, D. Harbottle, G.M. Kale, M.R. Tillotson, Synergistic effect of Fe and Ni on carbon aerogel for enhanced oxygen reduction and H2O2 activation in electro-Fenton process, Sep. Purif. Technol. 353 (2025) 128436, https://doi.org/10.1016/j.seppur.2024.128436.

[22] C. Yin, Y. Liu, X. Kang, X. Li, Synergistic degradation of tetracycline by CDs decorated g-C3N4 under LED light irradiation combined with the persulfate-based advanced oxidation process, Appl. Catal. A 636 (2022) 118571, https://doi.org/10.1016/j.apcata.2022.118571.

[23] R. Bardestani, G.S. Patience, S. Kaliaguine, Experimental methods in chemical engineering: specific surface area and pore size distribution measurements—BET, BJH, and DFT, Can. J. Chem. Eng. 97 (2019) 2781–2791, https://doi.org/10.1002/cjce.23632.

[24] N.A. Barakat, M. El-Newehy, S.S. Al-Deyab, H.Y. Kim, Cobalt/copper-decorated carbon nanofibers as novel non-precious electrocatalyst for methanol electrooxidation, Nanoscale Res Lett 9 (2014) 2, https://doi.org/10.1186/1556-276X-9-2.

[25] L.M. Pastrana-Martínez, A.M. Regadera-Macías, S. Morales-Torres, F.J. Maldonado-Hódar, Revisiting the influence of metals on resorcinol-formaldehyde carbon gels: physicochemical properties, transformations and synergism between phases, Inorg. Chim. Acta 535 (2022) 120850, https://doi.org/10.1016/j.ica.2022.120850.

[26] K. Xiao, X. Qi, Z. Bao, X. Wang, L. Zhong, K. Fang, M. Lin, Y. Sun, CuFe, CuCo and CuNi nanoparticles as catalysts for higher alcohol synthesis from syngas: a comparative study, Catal Sci. Technol. 3 (2013) 1591–1602, https://doi.org/10.1039/C3CY00063J.

[27] F.J. Maldonado-Hódar, C. Moreno-Castilla, J. Rivera-Utrilla, Y. Hanzawa, Y. Yamada, Catalytic graphitization of carbon aerogels by transition metals, Langmuir 16 (2000) 4367–4373, https://doi.org/10.1021/la991080r.

[28] L. Shang, X. Lv, H. Shen, Z. Shao, G. Zheng, Selective carbon dioxide electroreduction to ethylene and ethanol by core-shell copper/cuprous oxide, J. Colloid Interface Sci. 552 (2019) 426–431, https://doi.org/10.1016/j.jcis.2019.05.073.

[29] Z. Lu, G. Chen, S. Siahrostami, Z. Chen, K. Liu, J. Xie, L. Liao, T. Wu, D. Lin, Y. Liu, T.F. Jaramillo, J.K. Nørskov, Y. Cui, High-efficiency oxygen reduction to hydrogen peroxide catalysed by oxidized carbon materials, Nat. Catal. 1 (2018) 156–162, https://doi.org/10.1038/s41929-017-0017-x.

[30] M. Mohsenpour, S. Motahari, F. Tajabadi, M. Najafi, Preparation and application of sunlight absorbing ultra-black carbon aerogel/graphene oxide membrane for solar steam generation systems, RSC Adv. 10 (2020) 41780–41790, https://doi.org/10.1039/D0RA07522A.
[31] Y. Ping, Y. Zhang, Y. Gong, B. Cao, Q. Fu, C. Pan, Edge-riched graphene nanoribbon for high capacity electrode materials, Electrochim. Acta 250 (2017) 84–90, https://doi.org/10.1016/j.electacta.2017.08.051.
[32] S. Kundu, Y. Wang, W. Xia, M. Muhler, Thermal stability and reducibility of oxygen-containing functional groups on multiwalled carbon nanotube surfaces: a quantitative high-resolution XPS and TPD/TPR study, J. Phys. Chem. C 112 (2008) 16869–16878, https://doi.org/10.1021/jp804413a.
[33] H. Zhao, X. Shen, Y. Chen, S.-N. Zhang, P. Gao, X. Zhen, X.-H. Li, G. Zhao, A COOH-terminated nitrogen-doped carbon aerogel as a bulk electrode for completely selective two-electron oxygen reduction to H2O2, Chem. Commun. 55 (2019) 6173–6176, https://doi.org/10.1039/C9CC02580D.
[34] S. Wang, L. Zhang, Z. Xia, A. Roy, D.W. Chang, J. Baek, L. Dai, BCN graphene as efficient metal-free electrocatalyst for the oxygen reduction reaction, Angew Chem Int Ed 51 (2012) 4209–4212, https://doi.org/10.1002/anie.201109257.
[35] X. Sun, H. Qi, Z. Sun, Bifunctional nickel foam composite cathode co-modified with CoFe@NC and CNTs for electrocatalytic degradation of atrazine over wide pH range, Chemosphere 286 (2022) 131972, https://doi.org/10.1016/j.chemosphere.2021.131972.
[36] M.J. Pinzón C, J.M. de Aquino, R.G. Freitas, G.A. Pereira, L.M. Da Silva, H. Zanin, A comprehensive study about the influence of pore structures of carbon-based electrode materials on the charge-storage processes of water-in-salt based supercapacitors, J. Storage Mater. 62 (2023) 106858, https://doi.org/10.1016/j.est.2023.106858.
[37] Y.J. Sa, J.H. Kim, S.H. Joo, Active edge-site-rich carbon nanocatalysts with enhanced electron transfer for efficient electrochemical hydrogen peroxide production, Angew. Chem. Int. Ed. 58 (2019) 1100–1105, https://doi.org/10.1002/anie.201812435.
[38] J. Zhang, X. Song, P. Li, S. Wang, Z. Wu, X. Liu, An iron-based catalyst with multiple active components synergetically improved electrochemical performance for oxygen reduction reaction, Catalysts 8 (2018) 243, https://doi.org/10.3390/catal8060243.
[39] P. Cao, K. Zhao, X. Quan, S. Chen, H. Yu, Efficient and stable heterogeneous electro-Fenton system using iron oxides embedded in Cu, N co-doped hollow porous carbon as functional electrocatalyst, Sep. Purif. Technol. 238 (2020) 116424, https://doi.org/10.1016/j.seppur.2019.116424.
[40] K. Jiao, Z. Kang, B. Wang, S. Jiao, Y. Jiang, Z. Hu, Applying Co3O4@nanoporous carbon to nonenzymatic glucose biofuel cell and biosensor, Electroanalysis 30 (2018) 525–532, https://doi.org/10.1002/elan.201700719.
[41] Q. Ye, H. Xu, Q. Wang, X. Huo, Y. Wang, X. Huang, G. Zhou, J. Lu, J. Zhang, New insights into the mechanisms of tartaric acid enhancing homogeneous and heterogeneous copper-catalyzed Fenton-like systems, J. Hazard. Mater. 407 (2021) 124351, https://doi.org/10.1016/j.jhazmat.2020.124351.
[42] Y. Wu, T. She, Y. Wang, Z. Xu, T. Huang, Q. Ji, H. Song, S. Yang, S. Li, S. Yan, L. Zhang, H. He, Enhancing cationic superexchange interaction via adjustive lattice distortion in cobalt-based perovskite for improved Fenton-like decontamination, Appl. Catal. B 343 (2024) 123569, https://doi.org/10.1016/j.apcatb.2023.123569.
[43] Y. Gao, W. Zhu, J. Liu, P. Lin, J. Zhang, T. Huang, K. Liu, Mesoporous sulfur-doped CoFe2O4 as a new Fenton catalyst for the highly efficient pollutants removal, Appl Catal B 295 (2021) 120273, https://doi.org/10.1016/j.apcatb.2021.120273.
[44] S.K. Ling, S. Wang, Y. Peng, Oxidative degradation of dyes in water using Co2+/H2O2 and Co2+/peroxymonosulfate, J. Hazard. Mater. 178 (2010) 385–389, https://doi.org/10.1016/j.jhazmat.2010.01.091.
[45] T. She, Y. Wu, Q. Ji, Z. Xu, Y. Wang, H. Chu, Y. Liu, H. Song, S. Yang, S. Li, L. Zhang, H. He, Passivating surface states of graphitic carbon nitride for improved photocatalytic Fenton-like decontamination, Sep. Purif. Technol. 329 (2024) 125193, https://doi.org/10.1016/j.seppur.2023.125193.
[46] L. Wei, K. Zhou, H. Li, P. Yang, B. Liu, Cobalt based bimetallic catalysts for heterogeneous electro-Fenton adapting to vary pH for HEDP and MIT degradation, Environ. Technol. 1–12 (2024), https://doi.org/10.1080/09593330.2024.2356226.
[47] Y. Li, M. Yan, H. Lin, S. Wang, X. Duan, X.-L. Wu, Electrochemical generation of H*-•OH redox pair for rapid removal of refractory nitro-organic micropollutants, Appl. Catal.B: Environ. and Energy 361 (2025) 124663, https://doi.org/10.1016/j.apcatb.2024.124663.
[48] X. Shen, F. Xiao, H. Zhao, Y. Chen, C. Fang, R. Xiao, W. Chu, G. Zhao, In situ-formed PdFe nanoalloy and carbon defects in cathode for synergic reduction–oxidation of chlorinated pollutants in electro-Fenton process, Environ. Sci. Technol. 54 (2020) 4564–4572, https://doi.org/10.1021/acs.est.9b05896.
[49] F. Xiao, Z. Wang, J. Fan, T. Majima, H. Zhao, G. Zhao, Selective electrocatalytic reduction of oxygen to hydroxyl radicals via 3-electron pathway with FeCo alloy encapsulated carbon aerogel for fast and complete removing pollutants, Angew. Chem. Int. Ed. 60 (2021) 10375–10383, https://doi.org/10.1002/anie.202101804.
[50] Z. Xu, F. Zhang, W. Lin, H. Zhang, Polymer network-derived nitrogen/sulphur co-doped three-dimensionally interconnected hierarchically porous carbon for oxygen reduction, lithium-ion battery, and supercapacitor, RSC Adv. 9 (2019) 36570–36577, https://doi.org/10.1039/C9RA07619K.
[51] J. Lu, W. Hao, X. Wu, X. Shen, S. Cui, W. Shi, Electronic modulation of the 3D architectured Ni/Fe oxyhydroxide anchored N-doped carbon aerogel with much improved OER activity, Gels 9 (2023) 190, https://doi.org/10.3390/gels9030190.
[52] L. Yang, J. Shui, L. Du, Y. Shao, J. Liu, L. Dai, Z. Hu, Carbon-based metal-free ORR electrocatalysts for fuel cells: past present, and future, Adv. Mater. 31 (2019) 1804799, https://doi.org/10.1002/adma.201804799.
[53] C. Chen, Y. Zhu, M. Tian, Y. Chen, Y. Yang, K. Jiang, S. Gao, Sustainable self-powered electro-Fenton degradation using N, S co-doped porous carbon catalyst fabricated with adsorption-pyrolysis-doping strategy, Nano Energy 81 (2021) 105623, https://doi.org/10.1016/j.nanoen.2020.105623.
[54] L. Wang, Y. Zhou, J. Qiu, Influence of pore structures on the electrochemical performance of asphaltene-based ordered mesoporous carbons, Microporous Mesoporous Mater. 174 (2013) 67–73, https://doi.org/10.1016/j.micromeso.2013.02.024.
[55] Y. Chen, S. Ji, S. Zhao, W. Chen, J. Dong, W.-C. Cheong, R. Shen, X. Wen, L. Zheng, A.I. Rykov, S. Cai, H. Tang, Z. Zhuang, C. Chen, Q. Peng, D. Wang, Y. Li, Enhanced oxygen reduction with single-atomic-site iron catalysts for a zinc-air battery and hydrogen-air fuel cell, Nat. Commun. 9 (2018) 5422, https://doi.org/10.1038/s41467-018-07850-2.
[56] L. Yan, Y. Liu, J. Hou, High-efficiency oxygen reduction reaction revived from walnut shell, Molecules 28 (2023) 2072, https://doi.org/10.3390/molecules28052072.
[57] A. Lissaneddine, M.-N. Pons, F. Aziz, N. Ouazzani, L. Mandi, E. Mousset, A critical review on the electrosorption of organic compounds in aqueous effluent – Influencing factors and engineering considerations, Environ. Res. 204 (2022) 112128, https://doi.org/10.1016/j.envres.2021.112128.
[58] E. Rosales, S. Diaz, M. Pazos, M.A. Sanromán, Comprehensive strategy for the degradation of anti-inflammatory drug diclofenac by different advanced oxidation processes, Sep. Purif. Technol. 208 (2019) 130–141, https://doi.org/10.1016/j.seppur.2018.04.014.
[59] Business Electricity Rates UK, Business Electricity Prices (n.d.). https://www.businesselectricityprices.org.uk/ (accessed May 14, 2024).
[60] S. Han, Z. Wang, X. Pi, C. Wu, X. Wang, Y. Wang, X. Liu, H. Zhao, Promotion of tetracycline degradation by electro-Fenton: controlling the reaction zone by N-doped modified activated carbon cathode, J. Clean. Prod. 370 (2022) 133524, https://doi.org/10.1016/j.jclepro.2022.133524.
[61] A. Khan, Z. Liao, Y. Liu, A. Jawad, J. Ifthikar, Z. Chen, Synergistic degradation of phenols using peroxymonosulfate activated by CuO-Co3O4@MnO2 nanocatalyst, J. Hazard. Mater. 329 (2017) 262–271, https://doi.org/10.1016/j.jhazmat.2017.01.029.
[62] C. Qi, X. Liu, J. Ma, C. Lin, X. Li, H. Zhang, Activation of peroxymonosulfate by base: Implications for the degradation of organic pollutants, Chemosphere 151 (2016) 280–288, https://doi.org/10.1016/j.chemosphere.2016.02.089.
[63] Q. Ye, H. Xu, J. Zhang, Q. Wang, P. Zhou, Y. Wang, X. Huang, X. Huo, C. Liu, J. Lu, Enhancement of peroxymonosulfate activation for antibiotics removal by nano zero valent tungsten induced Cu(II)/Cu(I) redox cycles, Chem. Eng. J. 382 (2020) 123054, https://doi.org/10.1016/j.cej.2019.123054.
[64] X. Qin, P. Cao, X. Quan, K. Zhao, S. Chen, H. Yu, Y. Su, Highly efficient hydroxyl radicals production boosted by the atomically dispersed Fe and Co sites for heterogeneous electro-Fenton oxidation, Environ. Sci. Technol. 57 (2023) 2907–2917, https://doi.org/10.1021/acs.est.2c06981.
[65] J. Deng, J. Lu, Q. Yan, J. Pan, Basic research on chemical mechanical polishing of single-crystal SiC—Electro–Fenton: reaction mechanism and modelling of hydroxyl radical generation using condition response modelling, J. Environ. Chem. Eng. 9 (2021) 104954, https://doi.org/10.1016/j.jece.2020.104954.
[66] D. Kubo, Y. Kawase, Hydroxyl radical generation in electro-Fenton process with in situ electro-chemical production of Fenton reagents by gas-diffusion-electrode cathode and sacrificial iron anode, J. Clean. Prod. 203 (2018) 685–695, https://doi.org/10.1016/j.jclepro.2018.08.231.
[67] T. Yatagai, Y. Ohkawa, D. Kubo, Y. Kawase, Hydroxyl radical generation in electro-Fenton process with a gas-diffusion electrode: linkages with electro-chemical generation of hydrogen peroxide and iron redox cycle, J. Environ. Sci. Health A 52 (2017) 74–83, https://doi.org/10.1080/10934529.2016.1229935.
[68] S. Qiu, D. He, J. Ma, T. Liu, T.D. Waite, Kinetic modeling of the electro-fenton process: quantification of reactive oxygen species generation, Electrochim. Acta 176 (2015) 51–58, https://doi.org/10.1016/j.electacta.2015.06.103.
[69] T. Luo, H. Feng, L. Tang, Y. Lu, W. Tang, S. Chen, J. Yu, Q. Xie, X. Ouyang, Z. Chen, Efficient degradation of tetracycline by heterogeneous electro-Fenton process using Cu-doped Fe@Fe2O3: mechanism and degradation pathway, Chem. Eng. J. 382 (2020) 122970, https://doi.org/10.1016/j.cej.2019.122970.
[70] X. Zhou, D. Xu, Y. Chen, Y. Hu, Enhanced degradation of triclosan in heterogeneous E-Fenton process with MOF-derived hierarchical Mn/Fe@PC modified cathode, Chem. Eng. J. 384 (2020) 123324, https://doi.org/10.1016/j.cej.2019.123324.
[71] Y. Chai, P. Qin, Z. Wu, M. Bai, W. Li, J. Pan, R. Cao, A. Chen, D. Jin, C. Peng, A coupled system of flow-through electro-Fenton and electrosorption processes for the efficient treatment of high-salinity organic wastewater, Sep. Purif. Technol. 267 (2021) 118683, https://doi.org/10.1016/j.seppur.2021.118683.
[72] H. Qi, X. Sun, Z. Sun, Porous graphite felt electrode with catalytic defects for enhanced degradation of pollutants by electro-Fenton process, Chem. Eng. J. 403 (2021) 126270, https://doi.org/10.1016/j.cej.2020.126270.
[73] E. Brillas, I. Sirés, M.A. Oturan, Electro-Fenton process and related electrochemical technologies based on Fenton's reaction chemistry, Chem. Rev. 109 (2009) 6570–6631, https://doi.org/10.1021/cr900136g.
[74] Y. Yao, Y. Pan, Y. Yu, Z. Yu, L. Lai, F. Liu, L. Wei, Y. Chen, Bifunctional catalysts for heterogeneous electro-Fenton processes: a review, Environ. Chem. Lett. 20 (2022) 3837–3859, https://doi.org/10.1007/s10311-022-01453-6.
[75] G. Xia, Y. Lu, H. Xu, Electrogeneration of hydrogen peroxide for electro-Fenton via oxygen reduction using polyacrylonitrile-based carbon fiber brush cathode,

Electrochim. Acta 158 (2015) 390–396, https://doi.org/10.1016/j.electacta.2015.01.102.
[76] G. Lama, J. Meijide, A. Sanromán, M. Pazos, Heterogeneous advanced oxidation processes: current approaches for wastewater treatment, Catalysts 12 (2022) 344, https://doi.org/10.3390/catal12030344.
[77] J. Zhang, Y. Liu, J. Li, K. Wang, X. Zhao, X. Liu, Enhanced recovery of phosphorus from hypophosphite-laden wastewater via field-induced electro-Fenton coupled with anodic oxidation, J. Hazard. Mater. 464 (2024) 132750, https://doi.org/10.1016/j.jhazmat.2023.132750.
[78] F. Yu, M. Zhou, X. Yu, Cost-effective electro-Fenton using modified graphite felt that dramatically enhanced on H2O2 electro-generation without external aeration, Electrochim. Acta 163 (2015) 182–189, https://doi.org/10.1016/j.electacta.2015.02.166.
[79] C. Kuang, Y. Xu, W. Lai, G. Xie, Z. Pan, L. Zheng, M.P. Talawar, J. Ling, S. Ye, X. Zhou, Novel electrodes for cathode electro-Fenton oxidation coupled with anodic oxidation system for advanced treatment of livestock wastewater, Electrochim. Acta 321 (2019) 134605, https://doi.org/10.1016/j.electacta.2019.134605.
[80] M. Yu, H. Dong, K. Liu, Y. Zheng, M.R. Hoffmann, W. Liu, Porous carbon monoliths for electrochemical removal of aqueous herbicides by “one-stop” catalysis of oxygen reduction and H2O2 activation, J. Hazard. Mater. 414 (2021) 125592, https://doi.org/10.1016/j.jhazmat.2021.125592.